Linear properties of global energetic particle induced geodesic acoustic mode with bump-on-tail distribution in tokamak plasmas

Xijin Xiang and Guoyong Fu

Institute for Fusion Theory and Simulation

Department of Physics, Zhejiang University

Hangzhou, China

Abstract

A systematic study of Energetic particle-induced geodesic acoustic mode (EGAM) has been carried for bump-on-tail energetic distribution in tokamak plasmas using linear global hybrid simulation. The stability threshold of EGAM in energetic particle pressure is found to be very low. The eignemode structure becomes more and more radially extended as beam ion distribution evolves from bump tail distribution to fully slowing down distribution. The mode radial width increase with energetic particle gyroradius while the growth rate is maximized at $v/v_A = 0.3$.

INTRODUCTION

Energetic particle-induced geodesic acoustic mode (EGAM) [1, 2] is an n=0 axisymmetric mode driven by energetic particles. The mode frequency and mode structure are similar to those of geodesic acoustic mode (GAM) [3, 4]. It is mainly an electrostatic mode with the mode electric field having uniform toroidal and poloidal mode structure. However EGAM is qualitatively different from GAM since it has essential features of energetic particle mode (EPM) [5] with its mode frequency and radial structure determined non-perturbatively by energetic particles [1], i.e., the existence of EGAM is due to energetic particle effects. Energetic particle destabilization of GAM was first observed in JET where a fast-chirping n=0 mode was driven by ICRH-induced fast minority tail ions [6]. Subsequently a beam-driven GAM-like mode observed

in DIII-D was identified as EGAM [1, 2]. Both the measurement and theory show that the EGAM is a global mode with mode frequency inside the GAM continuum spectrum. Since then EGAM has been observed in other tokamaks [7-9] as well as in the Large Helical Device (LHD) [10-11]. Extensive theoretical and numerical work has been done on the linear physics of EGAM in the past decade [12-25]. The research on EGAM has been reviewed recently in several papers [26-28]. In particular much analytic and numerical work has been done on EGAM's linear stability and global mode structure with different energetic particle distributions. Local distribution relations have been analytically derived for slowing down distribution, shifted-Maxwellian distribution as well as bump-on-tail distribution. The original work of Fu [1] shows that, in the local limit for a slowing down anisotropic distribution, there exist 3 branches of modes: the GAM branch and two new EGAM branches, with only one mode can be unstable. The two EGAMs emerge when energetic particle pressure exceeds a threshold. For relatively small energetic particle speed ($\omega_{b0}/\omega_{GAM} < 1.4$ for the distribution considered), the EGAM branch with lowest frequency is unstable when energetic particle pressure exceeds a threshold. The mode frequency is lower than GAM's. On the other hand, for relatively large energetic particle speed ($\omega_{b0}/\omega_{GAM} > 1.4$), the GAM branch is destabilized by energetic particle without a threshold. The frequency of the GAM branch is also lower than GAM's at finite energetic particle pressure. For a simplified slowing down distribution with a single pitch angle, Qiu et al shows analytically that EGAM can be unstable for $\Lambda_0 B_0 > 2/5$ [22]. On the other hand, for a slowing down distribution with a loss cone in pitch angle, Berk and Zhou show that the loss cone distribution leads to fast excitation of EGAM right after NBI is turned on [12]. More recently bump-on-tail distributions have been considered to explain the high frequency branch of EGAM observed in LHD. It is shown that the high frequency branch of EGAM with frequency larger than GAM frequency is destabilized in LHD with a bump-on-tail distribution [21-22, 25].

In this work we investigate linear properties of global EGAM with bump-on-tail distribution in tokamak plasmas using kinetic-fluid hybrid simulations. We study systematically the mode properties such as mode frequency, mode stability and mode structure and their dependence on key energetic particle parameters. In particular we focus on global mode structure and difference between EGAM with a bump-on-tail distribution and that with slowing down distribution.

The paper is organized as follows. In Sec. II, we introduce the simulation model and the numerical method. In Sec. III, the EGAM frequency, growth rate and converged eigenmode in different physical conditions are described. In Sec. IV, the conclusions are given.

I. SIMULATION MODEL AND METHOD

Following the original work of Fu.[1], the system of equations for EGAM evolution are given below for the radial electric field perturbation E_r, the perturbed thermal plasma pressure δP_{th}, and the perturbed parallel and perpendicular energetic particle pressures $\delta P_{\parallel}$ and $\delta P_{\perp}$:

$$\frac{\partial}{\partial t}\left\langle \frac{\rho|\nabla r|^2}{B^2}\right\rangle E_r = \left\langle G(r,\theta)(\delta P_{\parallel} + \delta P_{\perp})\right\rangle \tag{1}$$

$$\frac{\partial}{\partial t}\delta P_{th} = 2\gamma G(r,\theta) P_{th} E_r \tag{2}$$

$$\delta P_{\parallel h} + \delta P_{\perp h} = \int d^3v (mv_{\parallel}^2 + \frac{1}{2}mv_{\perp}^2)\delta f \tag{3}$$

$$\frac{d\delta f}{dt} = -\frac{dE}{dt}\frac{\partial f_0}{\partial E} = -(mv_{\parallel}^2 + \frac{1}{2}mv_{\perp}^2)\frac{\partial f_0}{\partial E} G(r,\theta) E_r \tag{4}$$

where the bracket $\langle\rangle$ denotes the flux surface average, $G(r,\theta) = -(B_\phi R / JB^3)(\frac{\partial B}{\partial \theta})$ comes from geodesic curvature, ρ is plasma mass density, B is the equilibrium magnetic field strength, B_ϕ is the toroidal magnetic field, R is the major radius, J is the Jacobian of flux coordinates (r,θ,ϕ) with r being the radial flux variable (or minor radius). The subscript th denotes the thermal species, the subscript h denotes the energetic particle species, γ is coefficient of specific heat. δf is the perturbed energetic particle distribution, $f_0 = f_0(P_\phi, E, \mu)$ is the equilibrium distribution as function of constants of motion: P_ϕ the toroidal angular momentum, E the particle energy and μ the magnetic moment.

The first equation is derived from the flux the vorticity equation and the electrostatic approximation is assumed [1]. The second equation comes from the fluid model for thermal plasma. The last equation is derived from the drift kinetic equation where the property of P_ϕ being a constant of motion for n=0 mode has been used. The four equations form a self-consistent kinetic-fluid hybrid model for EGAM. The anisotropic equilibrium distribution function is adopted for energetic particles in this study:

$$f = \frac{cg(\bar{v})}{v^3 + v_c^3}\exp[-\frac{P_\phi}{e\Delta\Psi} - (\frac{\Lambda - \Lambda_0}{\Delta\Lambda})^2] \tag{5}$$

Where c is a constant coefficient in the equation , $P_\phi = e\Psi + mvR$ is the toroidal angular momentum, Ψ is the poloidal flux and v is the particle velocity, $\Lambda = \mu B_0 / E$ is the pitch angle which is the angle between the velocity of particles and local magnetic field, $\Delta\Psi$ is the radial width in the normalized poloidal flux, Λ_0 is the central pitch angle parameter. The parameters of anisotropic pitch angle distribution are $\Lambda_0 = 0.5$ and $\Delta\Lambda = 0.3$. $g(\bar{v})$ is a piece-wise linear function of the normalized particle velocity $\bar{v} = v / v_0$ with v_0 being the NBI injection speed and is defined as follows:

$$g(\bar{v}) = 0 \quad (\bar{v} < v_L - dv \text{ or } \bar{v} > 1 + dv) \tag{6}$$

$$g(\bar{v}) = \frac{\bar{v} - v}{dv} \quad (v_L - dv < \bar{v} < v_L) \tag{7}$$

$$g(\bar{v}) = 1.0 \quad (v_L < \bar{v} < 1.0) \tag{8}$$

$$g(\bar{v}) = 1 - \frac{\bar{v} - 1.0}{dv} \quad (1.0 < \bar{v} < 1 + dv) \tag{9}$$

Figure 1 plots $g(\bar{v})$ function.

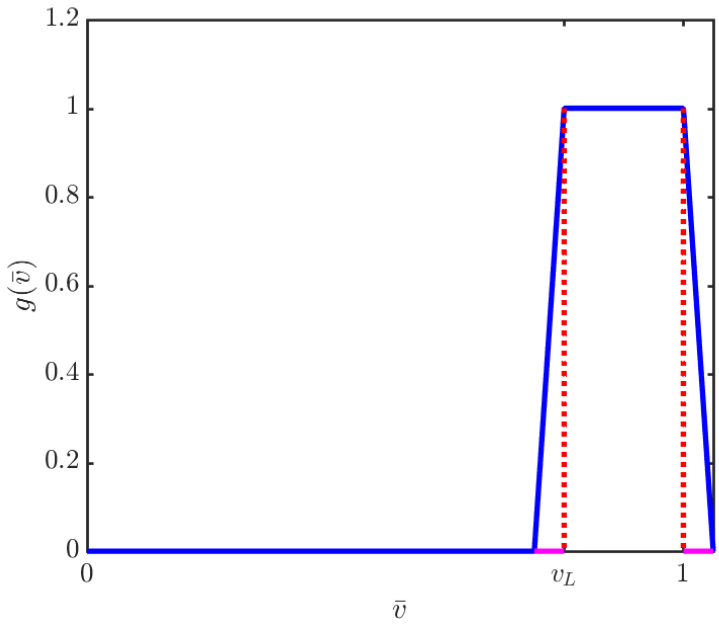

FIG. 1 $g(\bar{v})$ (blue solid line) vs $\bar{v}$ and the short pink lines is dv.

Where $dv = 1$ is a small parameter and is chosen to be $dv = 0.05$. The distribution f given in Eq. (5) is similar to the usual slowing down distribution used in the original work [1] and many other studies except for the extra velocity dependent factor $g(\bar{v})$. This factor models the beam ion distribution function from

starting of neutral beam injection to fully slowing down steady state distribution. The normalized velocity parameter v_L, which varies between dv and $1+dv$, controls the shape of velocity distribution during the slowing down process after NBI initialization. This distribution is a bump tail distribution when v_L is close to 1, and it is a fully slowing down one when $v_L = dv$.

II. SMULATION RESULTS

In this section, we present linear simulation results of global EGAM. The dependence of mode properties on energetic particle distribution will be discussed. In particular we will compare results with a bump-tail distribution with those with a slowing-down distribution.

The parameters used in our simulations are similar to those of DIII-D experiments [2]: the toroidal magnetic field $B_0 = 2T$, the major radius $R_0 = 1.7m$ and the plasma minor radius $a = 0.57m$. The plasma pressure profile is given by $P_{th} = P_{th}(0)(1-\Psi)$ with Ψ being the normalized poloidal flux. The safety factor profile $q = 3.9 - 1.89\Psi + 7\Psi^3$. The plasma density profile is assumed to be uniform for simplicity. For energetic particles, the energy of neutral beam injection is $E_{beam} = 75keV$. The corresponding beam ion injection velocity is $v_{beam}/v_A = 0.3$ with v_A is the Alfvén speed, the gyroradius defined with injection speed is $\rho_{beam}/a = 0.04$.

A. Dependence on distribution function: bump-tail versus slowing down

We have carried out linear simulation of EGAM with a scan of parameter v_L which controls the distribution function. Figure 2 shows the linear evolution of radial electric field E_r for the bump-tail distribution with $v_L = 0.95$. The horizontal axis is the normalized minor radius. The vertical axis is time in unit of Alfven time. We observe that the mode is linear growing with mode located mainly within about half minor radius.

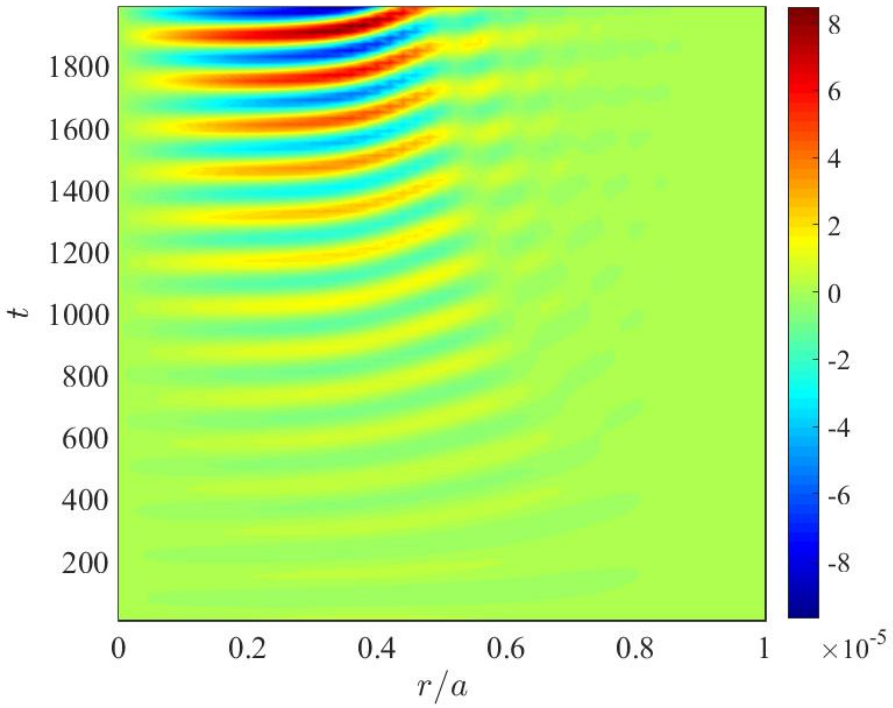

FIG. 2 The time evolution of radial electric field E_r for $v_L = 0.95$.

The linear simulations have carried out with a parameter scan in v_L values while keeping the coefficient c of the distribution in Eq.5 fixed, i.e., at constant injection power. Such parameter scan models the evolution of beam distribution starting from NBI turning on time in an experiment. The corresponding energetic particle pressure increases as v_L decreases from unit as shown in Fig. 4, where $Y = (P_{\parallel h} + P_{\perp h})/2P_{th}$ is the ratio of energetic particle pressure and thermal plasma pressure. The results of linear simulations with such a parameter scan are shown in Fig. 4 which plots mode frequency and growth rate as a function of v_L. As v_L decreases from unity, the mode frequency decreases and growth rate increases. The growth rate peaks at the intermediate value of $v_L = 0.6$ and then decreases to a finite value as v_L approach zero. These results are qualitatively consistent with the previous analytic theory [22].

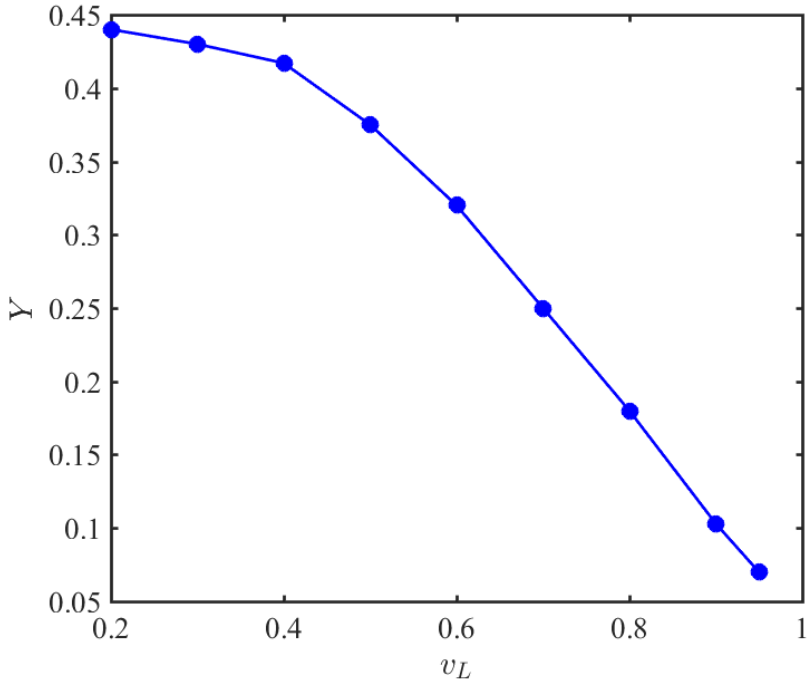

Fig. 3 The ratio of energetic particle pressure and thermal plasma pressure Y vs v_L

It should be noted that in our simulation, the normalized GAM frequency at the magnetic axis is $\omega_{GAM} = \sqrt{\gamma\beta_0} = 0.05$ based on the parameters of coefficient of specific heat $\gamma = 1.3$ and the thermal plasma central beta $\beta_0 = 0.2\%$. Thus our results indicate that the calculated mode frequencies of EGAM are always inside the GAM continuum spectrum which is shown in Fig. 5.

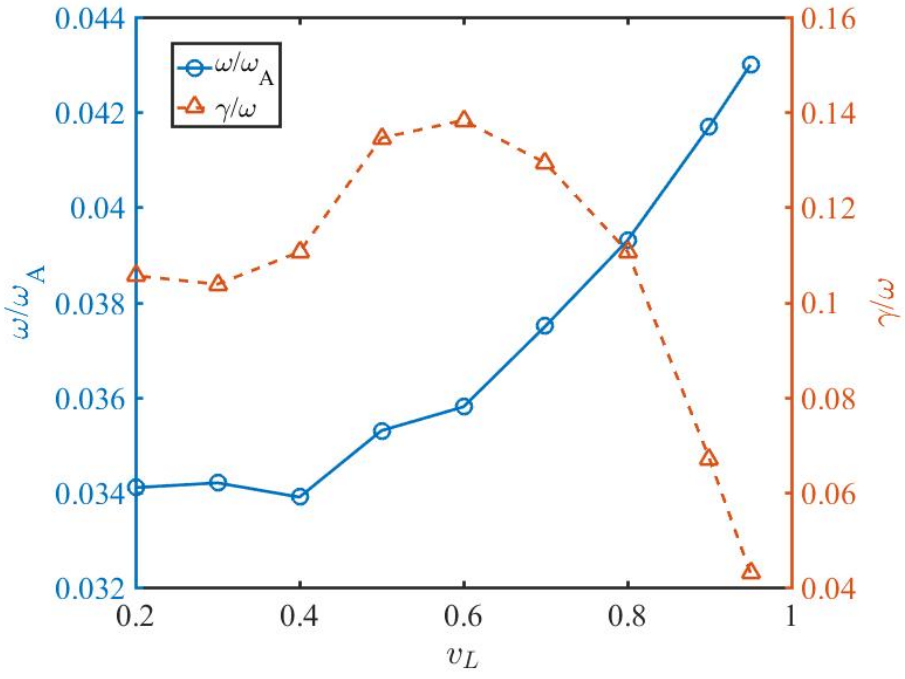

FIG. 4 Frequency (circles) and growth rate (rectangles) of EGAM versus v_L value.

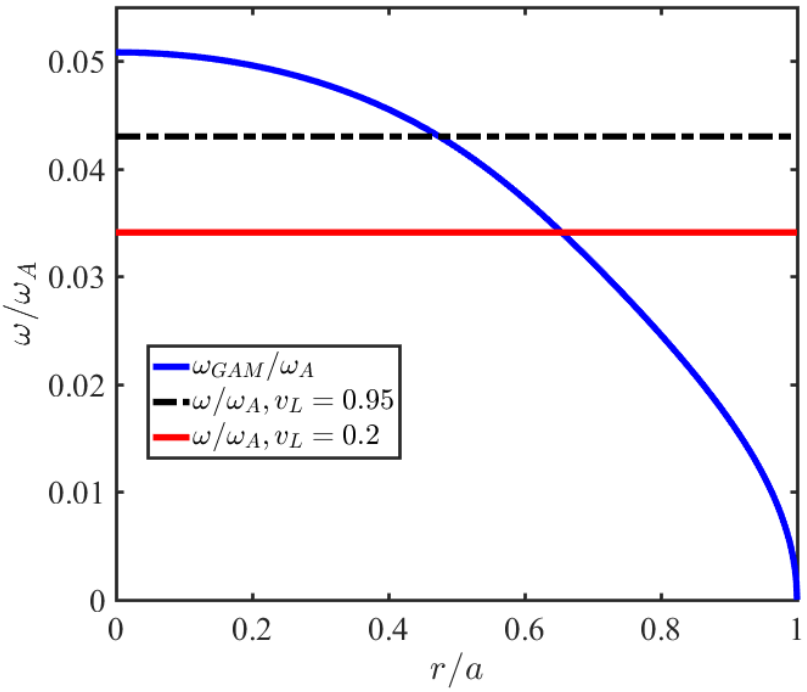

FIG.5 GAM continuum (blue solid line), simulation EGAM frequency for $v_L = 0.95$ (black dashed line) and for $v_L = 0.2$ (red solid line) versus normalized minor radius.

The EGAM frequency for $v_L = 0.95$, $v_L = 0.2$ and the GAM frequency versus normalized minor radius are shown in Fig. 5. The intersection point of GAM continuum and EGAM frequency for $v_L = 0.95$ is at $r/a = 0.48$, the other intersection point of GAM and EGAM frequency for $v_L = 0.2$ is at $r/a = 0.66$. According to Fig.6, we can see the mode structure peak is located in the left of intersection point. Fig. 6 plots the corresponding EGAM eigenmode structure for a sequence of v_L values. We observe that the mode structures are global. For $v_L = 0.95$, which corresponds to the bump-tail distribution, the mode structure is mostly located within half minor radius. As v_L decreases, the mode structure becomes more extended and more oscillatory. The peak of the mode moves from $r/a = 0.35$ to $r/a = 0.6$.

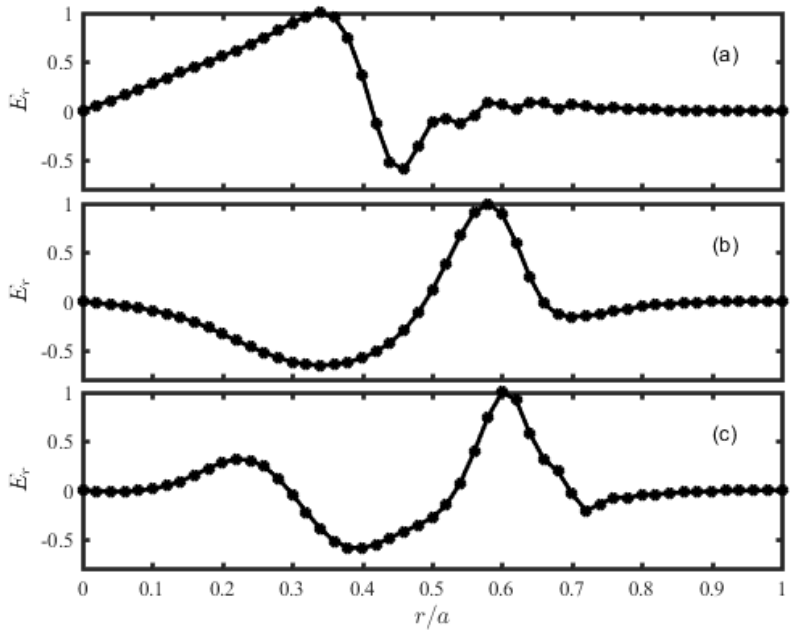

FIG. 6. The normalized eigenfunction E_r vs normalized minor radius r/a. (a) for $v_L = 0.95$; (b) for $v_L = 0.60$; (c) for $v_L = 0.20$.

B. Dependence on energetic particle pressure: stability threshold

We now investigate the dependence of EGAM frequency and growth rate on energetic particle pressure with the bump-on-tail EP distribution ($v_L = 0.95$). Fig. 7 shows the simulated mode frequency (solid blue line) and growth rate (dashed line). The solid red line is the fitted line for the growth. We find that the frequency decreases and the growth rate increases as Y increases. Extrapolating the growth rate to zero (solid red line) yield a critical value of energetic particle pressure $Y_{crit} = 0.02$ for excitation of EGAM. We have also examined the dependence on energetic particle pressure for the slowing down distribution ($v_L = 0.20$). The results are shown in Fig. 8. The corresponding stability threshold is $Y_{crit} = 0.12$ which is a factor of 6 larger than the one with the bump-tail distribution. The smallness of Y_{crit} for the bump-tail distribution implies fast excitation of EGAM after NBI heating is turned on. This result is consistent with observed fast excitation in the DIII-D experiments and is similar to the previous analytic results [12,22-23].

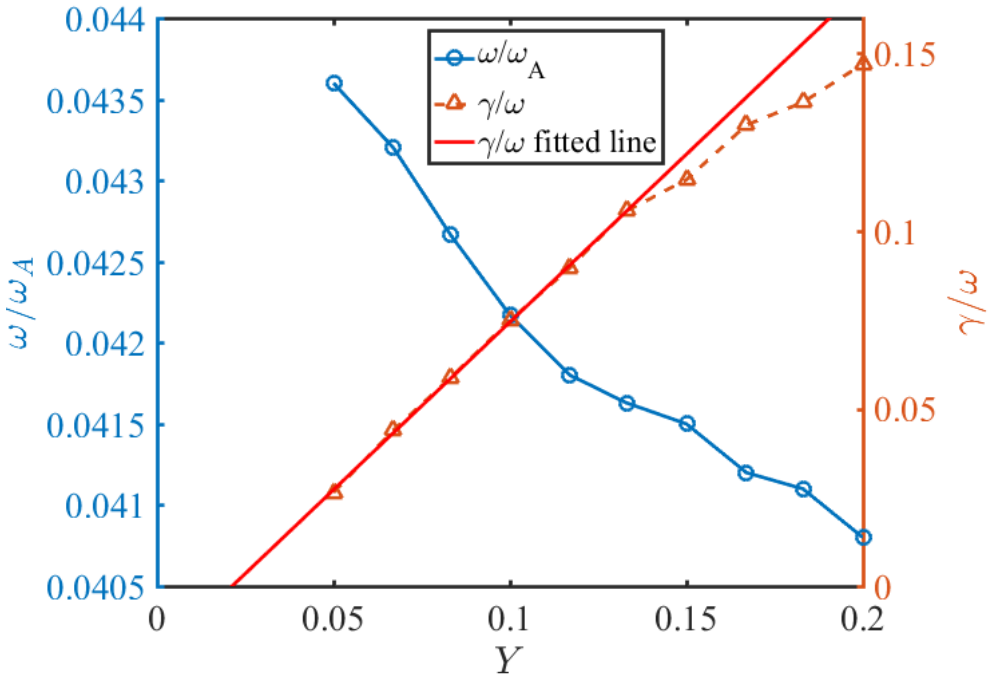

FIG. 7 Frequency (circles) and growth rate (rectangles) of EGAM vs $Y = (P_{\parallel h} + P_{\perp h})/2P_{th}$ for $v_L = 0.95$, the red line is the fitted line for the growth rate data.

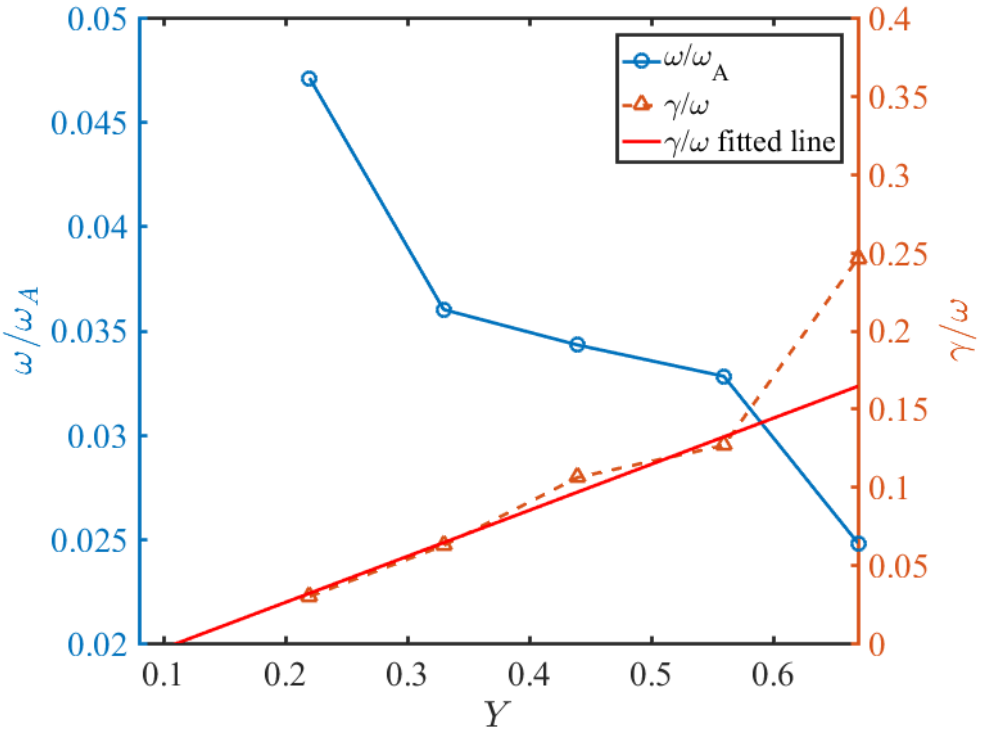

FIG. 8 Frequency (circles) and growth rate (rectangles) of EGAM vs $Y = (P_{\parallel h} + P_{\perp h})/2P_{th}$ for $v_L = 0.20$, the red line is the fitted line for the growth rate data.

C. Dependence on energetic particle speed

Fig. 9 shows the EGAM frequency and growth rate as a function of the normalized energetic particle speed for $v_L = 0.95$ and $Y = 0.0833$. The gyroradius of energetic particles is fixed at $\rho / a = 0.0358$. As expected the mode frequency increases with particle speed. However the dependence of growth rate is not monotonic. The growth rate is maximized at $v / v_A = 0.31$. Incidentally this value of particle speed coincides with the critical value of $Z = \omega_{b0} / \omega_{GAM} = 1.4$ at which the pattern of EGAM branches bifurcate [Fu's 2008 PRL].

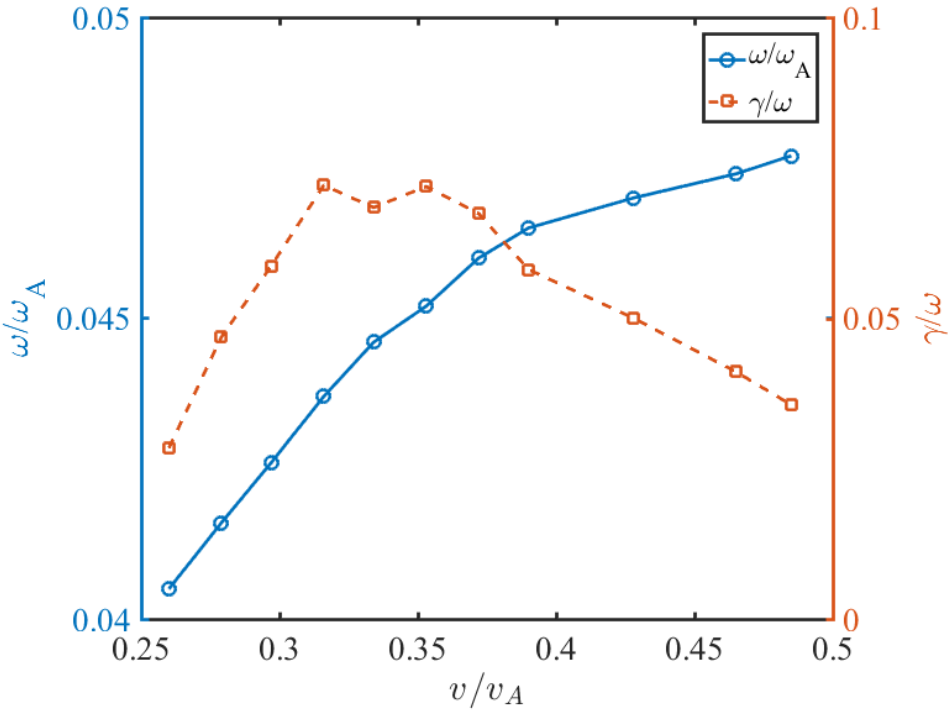

FIG. 9 Frequency (circles) and growth rate (rectangles) of EGAM versus energetic particle velocity for $v_L = 0.95$ and $Y = 0.0833$.

D. Dependence on energetic particle gyroradius

Fig. 10 shows the EGAM frequency and growth rate as a function of the normalized gyroradius at the fixed energetic particle speed $v / v_A = 0.03$, $v_L = 0.95$ and energetic particle pressure ratio $Y = 0.0833$. The results show that the mode frequency is nearly constant while the growth rate increases with ρ / a for $\rho / a > 0.03$. For smaller values of ρ / a, the growth rate is nearly constant. This is not surprising since the

growth rate is expected to converge to the local result as gyroradius approaches zero. We have also investigated the dependence of eigenmode structure on gyroradius. Figure 11 shows the EGAM mode structures for several values of ρ/a. We observe that the mode structure becomes narrower as ρ/a decreases consistent with theoretical prediction of Fu.

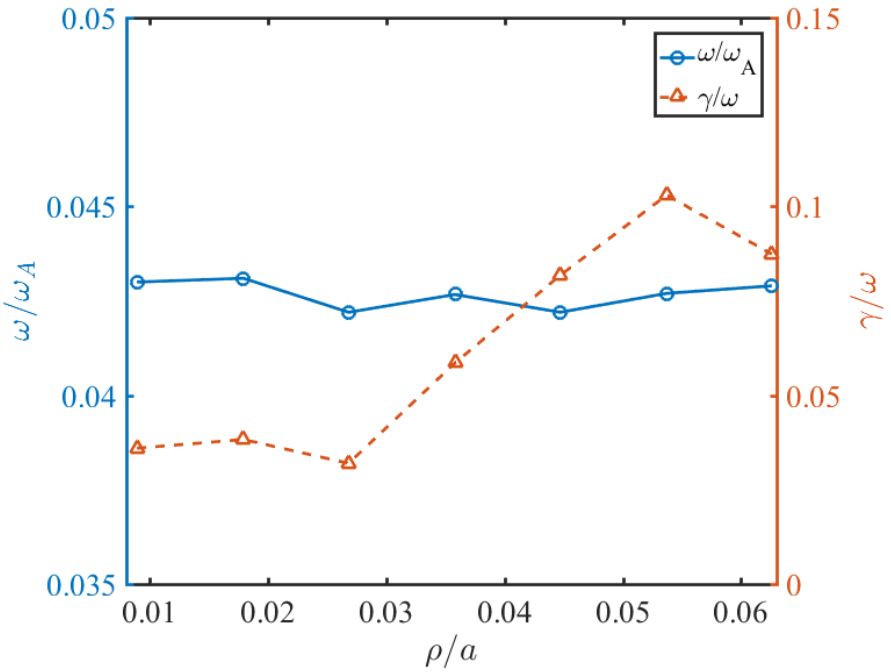

FIG. 10 Frequency (circles) and growth rate (rectangles) of EGAM versus energetic particle gyroradius for $v_L = 0.95$ and $Y = 0.0833$.

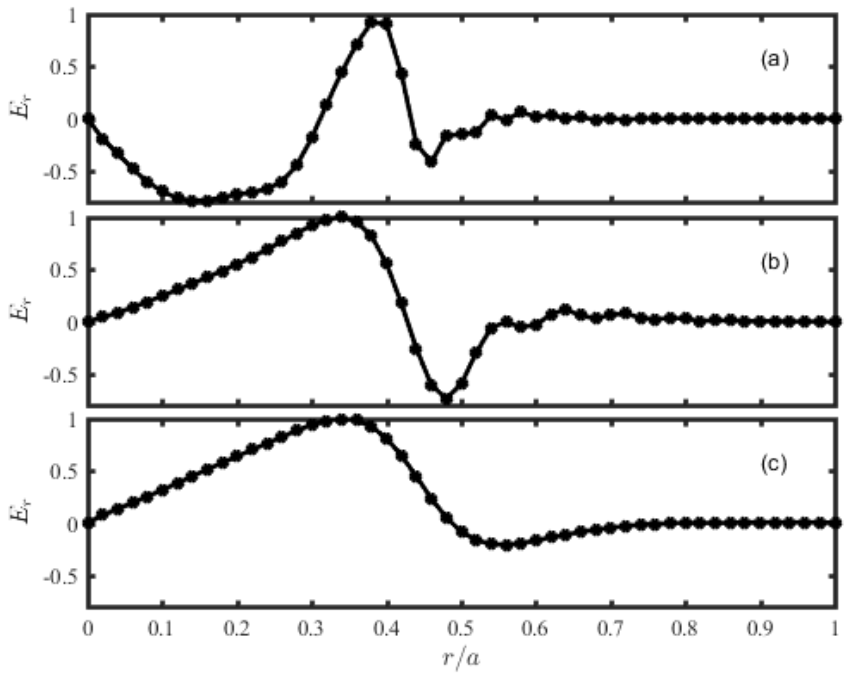

FIG. 11. The normalized eigenfunction E_r vs normalized minor radius r/a. (a) for $\rho/a = 0.0179$; (b)

for $\rho/a = 0.0358$; (c) for $\rho/a = 0.0537$.

E. Dependence on energetic particle pitch angle

Figure 12 shows mode frequency and growth rate as a function of central pitch angle parameter at a fixed energetic particle pressure $Y = 0.0833$. The mode frequency decreases as parameter increases as expected from theory since the particle parallel speed becomes smaller. However the growth rate dependence on parameter is more interesting. As parameter increases, the growth rate first decreases, and then increases and decreases again. It shows an oscillatory behavior.

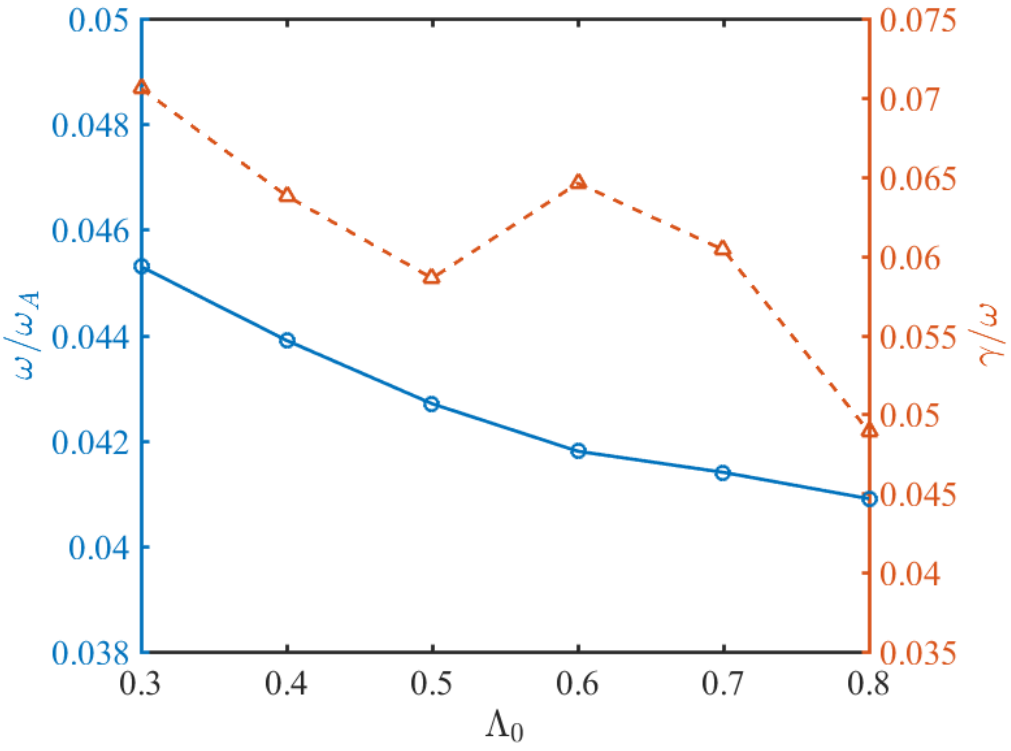

FIG. 12 Frequency (circles) and growth rate (rectangles) of EGAM versus pitch angle Λ_0 for $v_L = 0.95$ and $Y = 0.0833$.

III. Discussion and Conclusion

We have carried out a systematic study of linear properties of global EGAM in tokamak plasmas with parameters similar to those of DIII-D experiment where EGAM was observed. The hybrid model is used in simulations. In particular we focus on EGAM with a bump-tail beam ion distribution function formed

shortly after start of neutral beam injection before fully slowing down. Comparison between results of the bump tail and those of slowing down distribution shows that the EGAM's radial structure of the bump tail distribution is substantially less extended (contained mostly within half minor radius) while its frequency is about 25% higher. The EGAM stability threshold for the bump tail distribution is much lower. These results are consistent with experimental results of the DIII-D experiment. In addition, results of scan in energetic particle parameter show that both the mode growth rate and the mode radial width increases with gyroradius while the growth rate peaks at $v/v_A = 0.3$.

Our results are consistent with previous analytic and numerical studies. Comparing with the previous analytic local results of Cao [22] and Ren [25], our results are for global EGAM with a more realistic pitch angle distribution. Comparing with the previous global simulation work of Wang et al., our work considers parameters of a DIII-D like tokamak while their studies was focused on the high-frequency EGAM in LHD. In our work we investigate global EGAM systematically with an emphasis on global radial mode structure.

In conclusion, a systematic study of EGAM properties has been done for bump-on-tail energetic distribution in tokamak plasmas using linear global hybrid simulation. We find that the stability threshold in energetic particle pressure is very low implying fast excitation of EGAM after NBI is turned on. The EGAM becomes more and more radially extended as beam ion distribution evolves from bump-on-tail distribution to fully slowing down distribution. This prediction should be investigated experimentally in future.

REFERENCES

1. G. Y. Fu, Physical review letters **101** (18), 185002 (2008).

2. R. Nazikian, G. Y. Fu, M. E. Austin, H. L. Berk, R. V. Budny, N. N. Gorelenkov, W. W. Heidbrink, C. T. Holcomb, G. J. Kramer, G. R. McKee, M. A. Makowski, W. M. Solomon, M. Shafer, E. J. Strait and M. A. Zeeland, Physical review letters **101** (18), 185001 (2008).

3. N. Winsor, Physics of Fluids **11** (11), 2448 (1968).

4. P. H. Diamond, S. I. Itoh, K. Itoh and T. S. Hahm, Plasma Physics and Controlled Fusion **47** (5), R35-R161 (2005).

5. L. Chen L 1994 Phys. Plasmas 1 1519

6. H. L. Berk, C. Boswell , D. Borba, A. Figueiredo, T. Johnson, M. Nave, S. Pinches, S. Sharapov and

JET contributors, Nucl. Fusion 46, S888 (2006)

7. W. Chen *et al, Phys. Lett.* A **377,** 387 (2013)

8. L. Horváth, G. Papp, Ph. Lauber, G. Por, A. Gude, V. Igochine, B. Geiger, M. Maraschek, L. Guimarais, V. Nikolaeva, G.I. Pokol and the ASDEX Upgrade Team*, Nucl. Fusion* 56, 112003 (2016)

9. Ming Xu, Jizong Zhang, Tianchun Zhou, Yanmin Duan, Liqun Hu, Yingying Li, Liqing Xu, Tonghui Shi, Yong Liu, Songtao Mao, Juan Huang and The EAST Team *, Nucl. Fusion* 58, 096004 (2018)

10. K. Toi, M. Isobe, M. Osakabe, K. Ogawa, D. Spong, Y. Todo, and the LHD Experiment Group, Contrib. Plasma Phys. 50, No. 6-7, 493 – 500 (2010)

11. T. Ido, M. Osakabe, A. Shimizu, T. Watari, M. Nishiura, K. Toi, K. Ogawa, K. Itoh, I. Yamada, R. Yasuhara, Y. Yoshimura, S. Kato and The LHD Experiment Group, *Nucl. Fusion* 55, 083024 (2015)

12. Berk H and Zhou T 2010 Nucl. Fusion 50 035007

13. Qiu Z, Zonca F and Chen L 2010 Plasma Phys. Control. Fusion 52 095003

14. Qiu Z, Zonca F and Chen L 2011 Plasma Sci. Technol.

15. Qiu Z, Zonca F and Chen L 2012 Phys. Plasmas 19 082507

16. Zarzoso D, Garbet X, Sarazin Y, Dumont R and Grandgirard V 2012 Phys. Plasmas 19 022102

17. H. Wang, and Y. Todo, Physics of Plasmas **20**, 012506 (2013)

18. Wang H, Todo Y and Kim C C 2013 Phys. Rev. Lett. 110 155006

19. Kolesnichenko Y I, Lepiavko B S and Lutsenko V V, Plasma Phys. Control. Fusion 55 125007 (2013)

20. Biancalani A, Bottino A, Lauber P and Zarzoso D 2014 Nucl. Fusion 54 104004

21. Wang H, Todo Y, Ido T and Osakabe M 2015 Phys. Plasmas 22 092507

22. Cao J, Qiu Z and Zonca F 2016 Phys. Plasmas 22 124505

23. Qu Z S, Hole M J and Fitzgerald M, Phys. Rev. Lett. 116, 095004 (2016)

24. Qu Z S, Hole M J and Fitzgerald M, *Plasma Phys. Control. Fusion* **59,** 055018 (2017)

25. Haijun Ren and Hao Wang, Haijun Ren and Hao Wang, *Nucl. Fusion* **58,** 046005 (2018)

26. Zhiyong QIU, Liu CHEN and Fulvio ZONCA, *Plasma Sci. Technol.* **20,** 094004 (2018)

27. Chen L and Zonca F 2016 Rev. Mod. Phys. 88 015008